2018

Thulium Oxide Nanoparticles: A new candidate for image-guided radiotherapy

Elette Engels
University of Wollongong, ee215@uowmail.edu.au

Matt Westlake
University of Wollongong, mhw651@uowmail.edu.au

Nan Li
University of Wollongong, nli@uow.edu.au

Sarah Vogel
University of Wollongong, sv855@uowmail.edu.au

Quentin Gobert
Universite Versailles Saint-Quentin-En-Yvelines, quentin.gobert@u-psud.fr

See next page for additional authors

Thulium Oxide Nanoparticles: A new candidate for image-guided radiotherapy

Abstract

Nanoparticles, with their distinct properties that vary from their bulk material equivalent, continue to gain popularity for studies into multi-modal applications in medicine. This research introduces the use of thulium oxide nanoparticles for biological applications and characterizes the potential of this novel nanoparticle for image-guided radiotherapy of brain cancer. In this study, we investigate the structural characteristics of this nanoparticle, and reveal a significant dose enhancement towards radioresistant brain tumour cells *in vitro* that also underlies an improvement in the CT image contrast of brain tumours *in vivo*. The thulium oxide nanoparticles utilized in the investigations described in this article were measured to be 40–45 nm from x-ray diffraction and scanning electron microscopy data. *In vitro* investigations assessed the cell survival and DNA damage in 9 l gliosarcoma cells following irradiation with 150 kVp orthovoltage x-rays. Immediately after the 150 kVp irradiation (15 min) an increase in the number of γ-H2AX induced foci indicates the production of more double-strand DNA breaks. Following from the short time-frame irradiation outcomes, clonogenic cell survival assays confirmed long-term radio-sensitization, with the cell sensitivity increasing by a factor of 1.32 (measured at the 10% survival fraction) for the irradiated 9 l cells exposed to thulium nanoparticles. A simple CT experiment shows that our thulium nanoparticles suspended in water at concentrations >0.5 mg ml^{-1} (0.05–20 mg ml^{-1} investigated) are clearly observable against water. Extending the CT experiment to an *in vivo* investigation, cellular uptake of the nanoparticles was demonstrated through CT image enhancement of the cancer site in 9- to 10-week-old Fisher rats bearing 9 l gliosarcomas, 12 days after cell implantation. The 9 l cancer is clearly visible on the CT image after injecting 40 μg of nanoparticles (2 μl at 20 mg ml^{-1}) directly to the cancer site (5.5 mm from the dura and 3.5 mm right laterally of the bregma, 5 mm depth). To our knowledge, this work demonstrates the first application of thulium nanoparticles in biology and medicine, for radiotherapy and image guidance purposes.

Keywords

radiotherapy, image-guided, nanoparticles:, oxide, thulium, candidate

Disciplines

Engineering | Science and Technology Studies

Publication Details

Engels, E., Westlake, M., Li, N., Vogel, S., Gobert, Q., Thorpe, N., Rosenfeld, A., Lerch, M., Corde, S. & Tehei, M. (2018). Thulium Oxide Nanoparticles: A new candidate for image-guided radiotherapy. Biomedical Physics and Engineering Express, 4 (4), 044001-1-044001-11.

Authors

Elette Engels, Matt Westlake, Nan Li, Sarah Vogel, Quentin Gobert, Nathan Thorpe, Anatoly B. Rosenfeld, Michael L. F Lerch, Stephanie Corde, and Moeava Tehei

Thulium Oxide Nanoparticles: A new candidate for image-guided radiotherapy

Elette Engels[1,2], Matt Westlake[1,3], Nan Li[1,2], Sarah Vogel[1], Quentin Gobert[4], Nathan Thorpe[1], Anatoly Rosenfeld[1,2], Michael Lerch[1,2], Stéphanie Corde[1,2,5], Moeava Tehei[1,2]

[1] Centre for Medical Radiation Physics, University of Wollongong, NSW, Australia 2522
[2] Illawarra Health and Medical Institute (IHMRI), Wollongong, NSW, Australia 2522
[3] Institute for Superconducting and Electronic Materials, University of Wollongong, NSW Australia
[4] Université de Versailles Saint-Quentin-en-Yvelines, Versailles France, 78000
[5] Radiation Oncology Medical Physics, Prince of Wales Hospital, Randwick, NSW Australia

Corresponding Author: Moeava Tehei: moeava@uow.edu.au

ABSTRACT

Nanoparticles, with their distinct properties that vary from their bulk material equivalent, continue to gain popularity for studies into multi-modal applications in medicine. This research introduces the use of thulium oxide nanoparticles for biological applications and characterizes the potential of this novel nanoparticle for image-guided radiotherapy of brain cancer. In this study, we investigate the structural characteristics of this nanoparticle, and reveal a significant dose enhancement towards radioresistant brain tumour cells *in vitro* that also underlies an improvement in the CT image contrast of brain tumours *in vivo*. The thulium oxide nanoparticles utilized in the investigations described in this article were measured to be 40-45 nm from X-ray diffraction and scanning electron microscopy data. *In vitro* investigations assessed the cell survival and DNA damage in 9L gliosarcoma cells following irradiation with 150 kVp orthovoltage X-rays. Immediately after the 150 kVp irradiation (15 min) an increase in the number of γ-H2AX induced foci indicates the production of more double-strand DNA breaks. Following from the short time-frame irradiation outcomes, clonogenic cell survival assays confirmed long-term radio-sensitization, with the cell sensitivity increasing by a factor of 1.32 (measured at the 10% survival fraction) for the irradiated 9L cells exposed to thulium nanoparticles. A simple CT experiment shows that our thulium nanoparticles suspended in water at concentrations >0.5 mg/mL (0.05 – 20 mg/mL investigated) are clearly observable against water. Extending the CT experiment to an *in vivo* investigation, cellular uptake of the nanoparticles was demonstrated through CT image enhancement of the cancer site in 9- to 10-week-old Fisher rats bearing 9L gliosarcomas, 12 days after cell implantation. The 9L cancer is clearly visible on the CT image after injecting 40 µg of nanoparticles (2 µL at 20 mg/mL) directly to the cancer site (5.5 mm from the dura and 3.5 mm right laterally of the bregma, 5 mm depth). To our knowledge, this work demonstrates the first application of thulium nanoparticles in biology and medicine, for radiotherapy and image guidance purposes

INTRODUCTION

Brain and central nervous system (CNS) cancers are the leading cause of cancer-related death in children under the age of 10 (Australian Institute of Health and Welfare, 2017). While the 5-year survival rates for most cancers continue to improve, brain and CNS cancers have remained at 25% in Australia. These cancers often consist of highly radio-resistant cells, sub-categorized further as gliomas and glioblastomas (Kelley *et al* 2016). Gliomas represent approximately 30% of all cancers and 82% of malignant tumours in young adults, and yet survival for patients with brain cancer does not exceed 52% (Ostrom *et al* 2015). 9L gliosarcoma is an animal cell model similar to high-grade human glioma cells and shows a strong resistance to X-ray irradiation (Malaise *et al* 1986). 9L is the most widely used of all rat brain tumour models for research as well as a preclinical model used in brain radiotherapy and has been utilized in various treatment studies for over 30 years (Barth 1998).

In developed countries, radiation is used to treat half of all cancer patients (Baskar *et al* 2012). Photons generated by linear accelerators and X-ray tubes can be used to treat a broad range of tumours from deep-seated cancers to tumours on the surface of the skin, respectively. The success of cancer treatment with radiation depends on the total radiation dose delivered to a tumour and the tolerance of surrounding normal tissues (Barnett *et al* 2009). Radiation-induced damage occurs either directly or indirectly due to the production of ionising electrons and reactive oxygen species (ROS) respectively. The cellular response to radiation differs markedly however, due to location, function and more specifically, the repair mechanisms employed by the cell to correct radiation damage.

Equally important to the success of cancer treatment is the capability to image cancers, both for diagnosis and radiotherapy treatment planning purposes. Computed tomography (CT) is by far the most popular imaging modality that uses kilovoltage X-rays to contrast denser tissues against regions of lower density (Goldman, 2007). To help distinguish between tissues, contrast agents containing iodine (Z=53), are commonly used clinically. For well-vascularized tumour sites, contrast enhancement in tumours is possible. The passive uptake of iodinated molecules into tumours relies then on the vascularization and blood brain barrier permeability, location and hypoxic nature of the cells (Lusic *et al* 2013).

Nanoparticles ranging in size from 1 to 100 nm have gathered popularity for biological applications because their size allows them to pass easily into living cells, as well as their wide range in functionality (Hainfield *et al* 2004, 2008, Haume *et al* 2016, Maggiorella *et al* 2012, Retif *et al* 2015, Sinharay *et al* 2016). The field of nanomedicine extends to radiotherapy and diagnostic imaging, where high-Z nanoparticles are favoured for radiation technologies due to the strong Z-dependence of many photon interactions (Hainfeld *et al* 2008, Retif *et al* 2015). These nanoparticles produce more secondary electrons, auger electrons, ROS species, and characteristic X-rays that induce even more localized ionising radiation damage to cells and lead to radiosensitization. For use in the biological environment, biocompatibility and preferential cancer cell uptake also become useful properties for nanoparticle radio-sensitising agents. Nanomaterials which are the most commonly studied for use in radiotherapy or radiology include gold (Z=79). (Hainfeld *et al* 2008, Haume *et al* 2016, Retif *et al* 2015), hafnium (Z=72),

(Maggiorella *et al* 2012), and gadolinium (Z=64), (Kotb *et al* 2016), with many supporting reports on the success of these nanoparticles to increase local dose enhancement in tumours using kilo-voltage and mega-voltage radiation fields, with strong dependence on nanoparticle size, concentration, distribution, and beam energy.

Additional properties have been reported for nano-structured ceramics or metal oxide materials such as cerium oxide, bismuth oxide and tantalum oxide nanoparticles. Cerium oxide nanoparticles (Z= 58) have the unique ability to both radio-protect and radio-sensitize tumour cells depending on beam energy (Briggs *et al* 2013). Bismuth (Z= 83) oxide nanoparticles show selective toxicity towards radioresistant gliomas (Bogusz *et al* 2014, Stewart *et al 2016*) and tantalum oxide (Z=73) nanoparticles exhibit preferential uptake into tumours, low toxicity, a unique ordering around the cell nucleus, and are shown to radio-sensitize glioma cells (Brown *et al* 2014, 2016, McKinnon *et al* 2016, McDonald *et al* 2018). High-Z tantalum pentoxide nanoparticles produce a sensitivity enhancement ratio (SER) at 10% surviving fraction of 1.33 ± 0.07 with both mega voltage (Brown *et al* 2014) and kilovoltage (Brown *et al* 2016) treatments.

Aside from radiotherapy, high-Z nanoparticle materials such as gold (Ashton *et al* 2015 and McQuaid *et al* 2016), gadolinium (Sinharay *et al* 2016, Lohrke *et al* 2016) and bismuth oxide (Bogusz *et al* 2014, Stewart *et al* 2016) are shown to be successful candidates for imaging techniques such as computed tomography. Circulation half-lives have been reported to be 15 hours for high-Z nanoparticles, whereas iodine-based molecules half-lives dissipate within minutes (Ashton *et al* 2015).

Lanthanide nanoparticles commonly used for image-guidance include gadolinium. Gadolinium-based nanoparticles have been used in patients since 1988 for Magnetic Resonance Imaging (MRI) (Lohrke *et al* 2016) and researched for CT since 1980 (Havron *et al* 1980). With strong potential for many imaging and therapeutic modalities, these nanoparticles are now gaining popularity for image-guided radiotherapy. AGuIX®, a gadolinium-based nanoparticle, is one candidate that has now reached clinical trials (Maggiorella *et al* 2012).

There are however, some concerns over the toxicity of some gadolinium-based agents. The chance of nephrogenic systemic fibrosis (NSF), a potentially fatal disorder in patients with renal disease, was first linked directly to gadolinium-based contrasts in 2006. The primary categories of gadolinium-based nanoparticles are macrocyclic and linear. Macrocyclic structures encase gadolinium within complex cavities, which results in a more stable system, less likely to release free gadolinium to the body (Rogosnitzky *et al* 2016). The linear form has caused some concern recently due to the lower stability of this gadolinium-based agent in the body, prompting a removal from market in Europe (European Medicines Agency, 2017). Due to this, the potential of new paramagnetic nanoparticles for applications in imaging and radiotherapy must now be considered.

Thulium is a rare earth metal that has no known biological application to date. Thulium presents a higher atomic number than gadolinium (Z=69) and exhibits paramagnetic properties (Koehler *et al* 1962), which could lead to applications in CT and magnetic resonance imaging respectively.

Thulium is used predominately in lasers, (in this case created by bombarding thulium-169 in a nuclear reactor with neutrons to make a portable radiation source), and it is gaining popularity for the surgical treatment of benign prostate obstructions from 2005 (Barbalat *et al* 2016). Thulium-based or thulium doped nanoparticles exist in bio-photonics field with potential applications in luminescent nanothermometers, high resolution bio-imaging, and hyperthermia for diagnosis and therapy of diseases (Heiligtag and Niederberger 2013, Pereira *et al* 2017).

Thulium oxide is less frequently studied; however there are some noted applications of thulium oxide in X-ray devices, phosphors, atomic reactors, medicine, and semiconductors (Sidorowicz *et al* 2016). Thulium oxide nanoparticles in particular, can be also used in the fabrication of an electrochemical glucose biosensors (Zhang *et al* 2011).

With growing requirements for improving the shortcomings of radiotherapy and imaging modalities, much of the research is placed in novel theranostic agents, of which high-Z nanoparticles are a prominent subject of interest. Thulium and other lanthanide-based nanoparticles become promising candidates for use in both imaging and radiotherapy. In this article, we introduce thulium oxide nanoparticles as a potential candidate for image-guided radiotherapy and this is to our knowledge the first biological application of thulium oxide nanoparticles.

METHODS AND MATERIALS

Nanoparticle Preparation and Characterization

Thulium (III) oxide nanoparticles (99.9% trace metals basis) were obtained from Sigma Aldrich. For initial characterization, a sample of the thulium oxide nanoparticles were analysed with X-ray diffraction (XRD) using a GBC MMA X-ray diffraction system scanning between 20 to 90 degrees to determine structural information and mean particle size. The nanoparticle sample was exposed to Cu K-alpha radiation with wavelength $\lambda = 1.5418$ Å, accelerating voltage 40 kVp and cathode current 30 mA.

For further confirmation of the nanoparticle size, high-resolution transmission electron microscopy (HR-TEM) images were obtained. The thulium nano-powder sample was crushed with mortar and pestle then sonicated in ethanol/water for 40 minutes. The resulting mixture was then added drop wise onto a Holly carbon mesh covered copper grid. A JEOL JEM-ARM200F was used to acquire images with an accelerating voltage of 200 kV. Scanning electron microscopic (SEM) images were acquired on a JEOL JSM-7500FA SEM with analysis of particle size completed in Image J. Pixel length of the particles was measured and then normalized to a known scale of 100 nm.

Cell Culture and Nanoparticle Cytotoxicity

9L gliosarcoma cells (obtained from the European Collection of Cell Cultures (ECACC)) were cultured in T75cm^2 flasks containing complete Dulbecco's modified eagle medium (c-DMEM

from Gibco, also including 10% foetal bovine serum (FBS) and 1% penicillin and streptomycin (PS)) and incubated at 37°C and 5% (v/v) CO_2.

Before the addition of nanoparticles or treatment with radiation, 9L gliosarcoma cells were sub-cultured into T12.5cm^2 flasks (BD Falcon^{TM}) containing complete DMEM.

Thulium oxide nanoparticles were sonicated for 30 mins in DPBS (Dulbecco's phosphate buffer solution, Ca2+/Mg2+ free, Gibco BRL, AUS), to separate particles using a Branson Ultrasonic water bath. Various concentrations (50 - 200 μg/mL) were added to independent T12.5cm^2 flasks 24 hrs before the cells reached 95-100% confluence.

Cytotoxicity was determined by a clonogenic assay following the 24 hrs incubation of the 9L cells with the nanoparticles. Cells were washed with DPBS and trypsinized before seeding into 100 mm petri dishes that contained 10 mL of complete DMEM . Each independent flask was seeded in triplicate sets corresponding to each treatment including the controls with 0 μg/mL of nanoparticles. After 15 doubling times, each dish was washed with 5 mL DPBS (with Ca^{2+}/Mg^{2+}) and stained with solution crystal violet solution of 1:3 (v/v) in 70% ethanol, from a 2.3% crystal violet stock (Sigma Aldrich). The surviving colonies of 50 cells or more were counted and compared with the initial seeding number to determine the plating efficiency (PE). For each group, the surviving fraction (SF) was calculated by taking the ratio of the PE of the irradiated cells, by the PE of the non-irradiated control.

Cell Irradiation

The irradiation of 9L cells was performed at Prince of Wales Hospital (Randwick, NSW, Australia) using a Nucletron Oldelft Therapax DXT 300 Series 3 Orthovoltage X-ray machine (Nucletron B.V., Veenendaal, The Netherlands). T12.5cm^2 flasks containing monolayer of 9L under 6 mm of complete medium were irradiated horizontally at a distance of 50 cm from the source in full scatter conditions including solid water below and adjacent to cells. X-rays were generated at 150 kVp with a beam current of 20 mA using inherent filtration of 3 mm Be and additional 0.35 mm of copper and 1.5 mm of aluminium (HVL= 0.68 mm Cu). These X-rays were used to irradiate the cells with a dose rate of 0.754 Gy/min for doses ranging from 1 to 8 Gy at 6 mm depth. The beam effective energy was chosen to better target the maximum in mass energy absorption coefficient thulium oxide relative to water (Figure 1).

9L cells reached 95-100% confluence in T12.5cm^2 flasks prior to treatment. Cells were irradiated with and without thulium oxide nanoparticles that were added in a concentration of 50 μg/mL 24 hrs before irradiation. Clonogenic assay was the radiobiological endpoint to quantify the cells survival.

The surviving fraction of cells is known to follow a linear quadratic model (Jones *et al* 2001) which was fitted to the curve representing the surviving fraction of the cells and its dependence on the irradiation dose:

$$SF = \exp\left(-(\alpha D + \beta D^2)\right) \quad (1)$$

Here, D (Gy) is the irradiation dose and α (Gy^{-1}) and β (Gy^{-2}) are parameters representing direct lethal and sub-lethal damage, respectively.

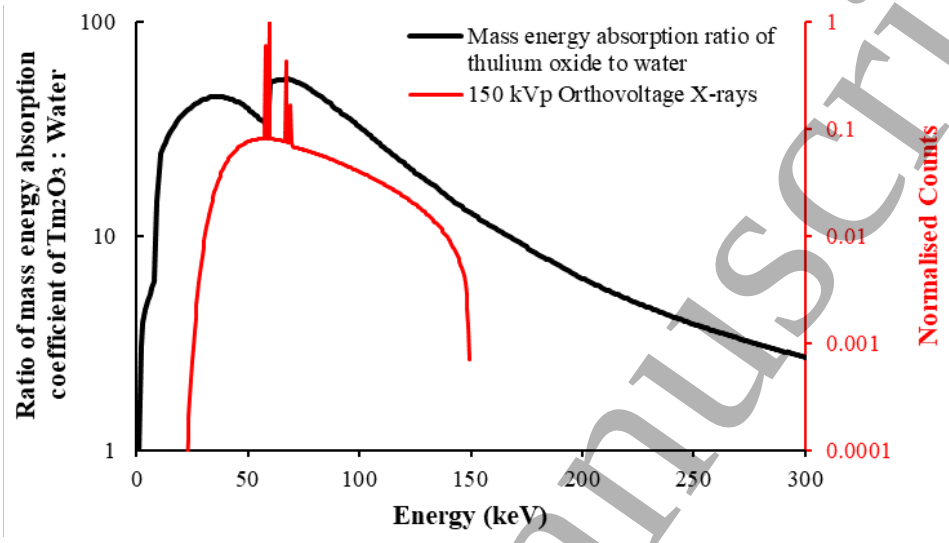

Figure 1: The ratio of the mass energy absorption coefficients of thulium oxide to water (Nowotny, 1998) is overlayed with the 150 kVp orthovoltage X-ray energy spectrum produced by SpekCalc (Poludniowski *et al* 2009). The X-ray spectrum has been normalized to the most probable energy count in the spectrum.

DNA double-strand breaks were revealed by γ-H2AX detection (Ivashkevich *et al* 2012). Following the irradiation of the 9L cells *in vitro* as described above, for the case with and without nanoparticles, the cells were incubated at 37oC and 5% CO2 (v/v) for 15 mins. After incubation, 9L cells were fixed with 100% ice-clod methanol for 20 mins and washed with ice-cold DPBS three times. The flasks were treated twice with blocking solution of 3% BSA (bovine serum albumin) in DPBS. A primary antibody (Mouse anti-phospho-Histone H2AX, at Ser139 clone JBW301) was added 1:500 in 1% BSA DPBS to the cells, and cells were incubated for 2 hours. The cells were washed with DPBS to remove the primary antibody before a secondary antibody (goat anti-Mouse IgG1 Cross-Absorbed, Alexa Fluor 488) was added 1:500 in 1% BSA DPBS and incubated for 1 hour in darkness. Lastly, cells were washed in DPBS and images acquired with a Leica DMi8 fluorescent microscope with a 40x water immersion objective and 20x dry objective. The images were analysed on the Leica Application Suite X (LAS X) software and ImageJ.

Flow Cytometric Measurement of Tm_2O_5 Internalization

Thulium oxide nanoparticles were exposed to cells for 24 hrs in T12.5cm^2 flasks, under the aforementioned cell growth conditions. Cells were washed with DPBS, trypsinized and harvested

before centrifuging at 380 g for 5 mins at room temperature. The cells were then washed twice with DPBS, before resuspension in DPS with a concentration of 10^6 cells/mL. A BD LSRFortessa™ flow cytometer analysed the cell sample to measure forward scatter (FSC) and side scatter (SSC).

CT Imaging

Thulium nanoparticles of concentrations 0 – 20 mg/mL in DPBS were transferred to 5 mL Eppendorf tubes and imaged using a Toshiba Asteon CT scanner with 1 mm slice thickness obtained at 100 kVp energy and 50 mA beam current. Hounsfield units (HU) of each sample were measured using ImageJ. For comparison with the NPs in solution, expected CT numbers and electron density of known materials were obtained from a Gammex 467 Tissue Characterization Phantom.

In vivo experiments were performed in an implanted 9L gliosarcoma tumour in the brain of 5 male Fischer rats. Fischer rats were obtained from the Animal Resource Centre (ARC) in Perth, Australia, and housed in individually ventilated cages with 3 rodents per cage. At 8 weeks old, 10^3 9L cells were injected 3.5 mm to the lateral right of the bregma midline intersection and at 5.5 mm depth from the dura into the caudate nucleus of the brain. Rodents were maintained at 2-3% isoflurane during surgery and provided with buprenorphine orally before and after surgery (0.4 mg/kg). Bupivacaine was administered directly to the scalp before injection (7 mg/kg) as a local anaesthetic. After 12 days following tumour cell injection, rats were maintained at 2-3% isoflurane with the same methods for pain relief, for the injection of thulium oxide nanoparticles into the tumour via the same burr hole at 5.5 mm depth, with a concentration of 20 mg/mL and a volume of 1.8 μL. CT images were obtained using a Toshiba Asteon CT with 1 mm slice thickness and beam energy and current of 100 kVp and 200 mA respectively. Images were acquired at 5 mins, 10 mins, and 25 mins, and from 8 to 24 hrs following nanoparticle injection to investigate the uptake, distribution, and evacuation of the thulium oxide nanoparticles. All operative procedures and animal care were in conformity with the guidelines of the Australian Government code for the care and use of animals for scientific purposes and under the approval of the University of Wollongong animal ethics committee agreement (AE16/12).

RESULTS

Nanoparticle Structural Characterization

Structural information and the average size of thulium oxide nanoparticles were measured using XRD and confirmed with SEM and TEM images. XRD measurements of the thulium oxide nanopowder are shown in Figure 2. Analysis of peaks present indicate that the material is single phase and a body-centred cubic structure, which is in good agreement with the PDF card number 10-0350. Further fitting and refinement in MAUD (Materials Analysis Using Diffraction, Lutterotti *et al* 1997) gave the crystalline parameter a = (10.495 ± 0.016)Å. The mean crystallite size was determined to be 42.52 nm using Tracers V6.6.9 which employs Scherrer's equation

(Borchertt *et al* 2005) to calculate the crystalline size. The size of the nanoparticles was confirmed to be 40nm – 45nm on average with SEM images. A HR-TEM image shows a sample of the nanoparticle sizes in Figure 3.

The particle size of thulium oxide nanoparticles may indicate a greater likelihood to be taken up into cells, following a review of nanoparticle size-dependence on cellular uptake that finds nanoparticles with sizes of approximately 50 nm are shown to have the greatest potential to be internalized into the cell (Shang *et al* 2014).

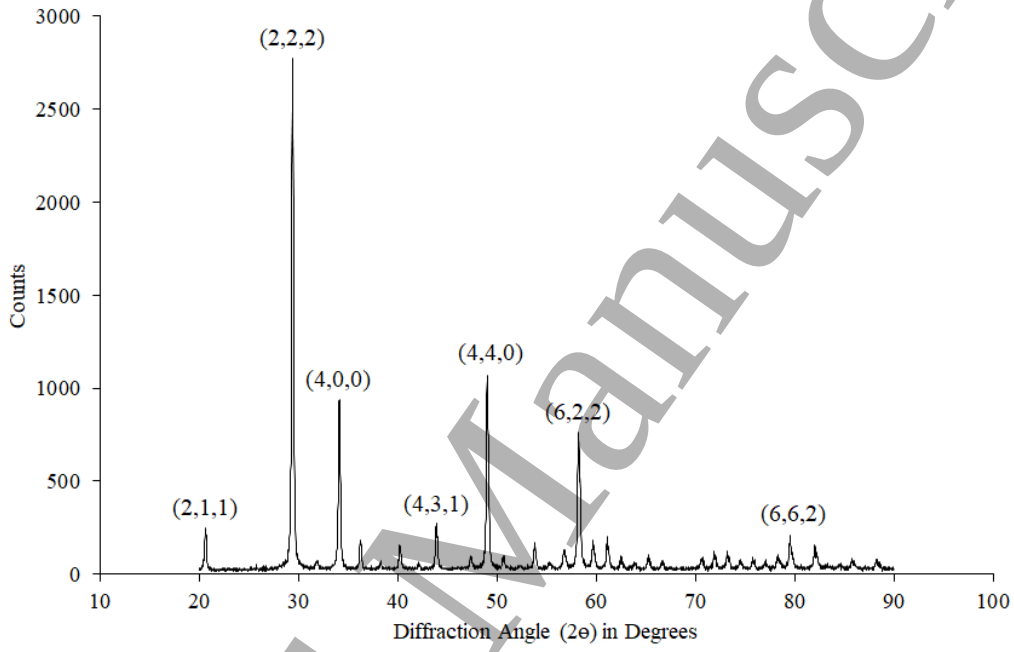

Figure 2: Thulium oxide nano-powder XRD, showing major peaks of reflection and corresponding Miller indices.

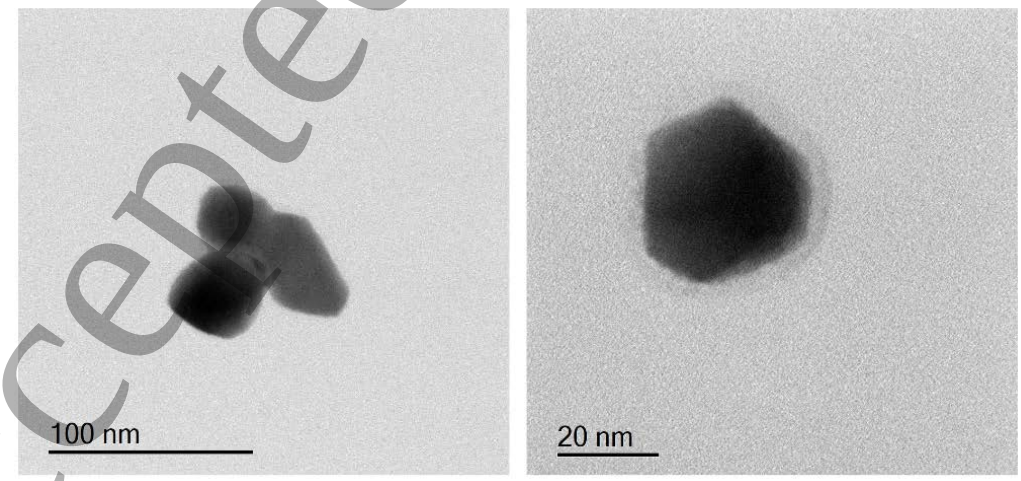

Figure 3: HR-TEM image showing morphology of thulium oxide nanoparticles on a 100 nm and 20 nm scale.

Nanoparticle Internalization and Cytotoxicity Measurements

After 24 hrs of incubation with thulium oxide nanoparticles, the cells were analysed to determine the change in mean side scatter (SSC) and forward scatter (FSC) in the presence of nanoparticles as an indication of NP uptake by the cells. Figure 4 shows the trend of the SSC dependence on FSC for the case with and without NPs. Gating has been applied between 35 to 135 from the FSC area (FSC-A) in order to exclude cell debris.

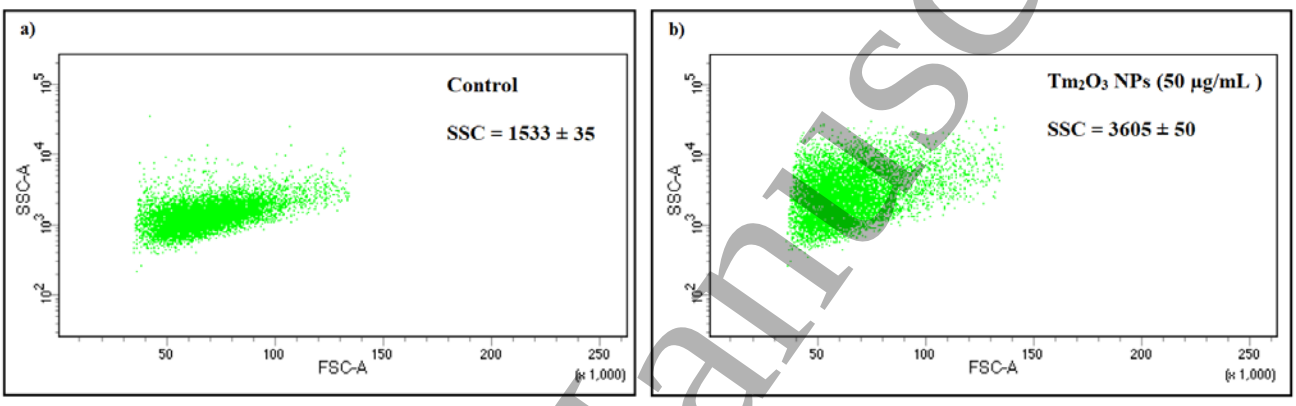

Figure 4: Flow cytometric measurements of 9L gliosarcoma cells indicating the internalization of Tm_2O_3 cells in terms of SSC magnitude. A control set (a) consisting of 9L cells only is compared with 9L cells that have been incubated with NPs for 24 hrs at a concentration of 50 µg/mL (b).

While the size of the cell can be related to the forward scatter of light, the amount of side scattered light from internal components within the cells can be related directly to the number of internalized nanoparticles within the cell. Figure 4 shows an increase in the mean side scatter due to the presence of Tm_2O_3 NPs by 2.35 times the original SSC of the control. From this, we conclude that nanoparticles have been internalized into the 9L cells. We can attribute this to the nanoparticle size and the shape. According to Kinnear *et al* 2016 nanoparticle shape is equally important in the method and speed of uptake. Smaller spherical particles or those with larger surface area are often linked to better interaction with the cell membrane and are involved in clathrin-mediated endocytosis as a form of internalization as well as macropinocytosis for larger particles. We hypothesise these are the main methods of internalization of these particles along with more phagocytotic mechanisms which we have observed in 9L.

Toxicity of the NP was assessed by clonogenic survival of 9L cells incubated with different concentrations of thulium oxide nanoparticles as shown in Figure 5. Mean survival values were obtained from at least three independent experiments for clonogenic assay experiments. Errors are calculated from the standard deviation of the mean.

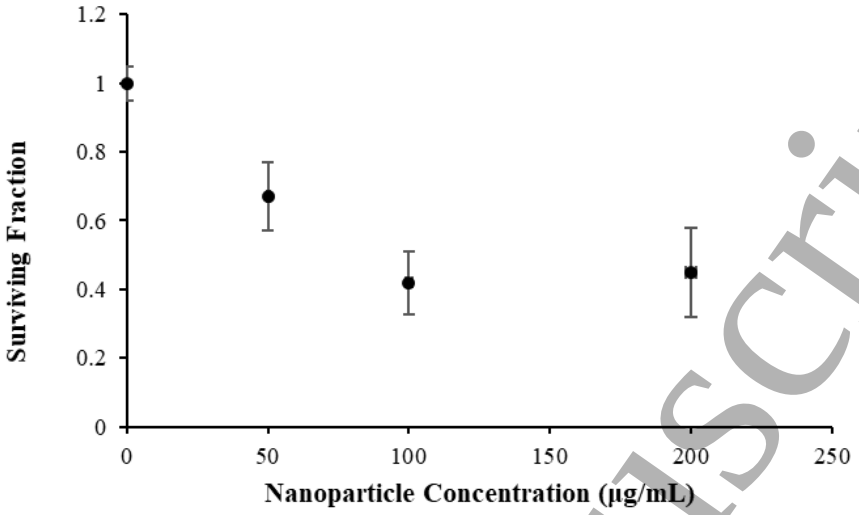

Figure 5: Clonogenic survival of 9L gliosarcoma cells exposed to different concentration of Thulium oxide.

After 24 hrs of exposure, the thulium oxide NPs are internalized into the cell and as a result, there is a reduction in the cell survival of 9L gliosarcoma. The toxicity towards the 9L cancer cells tends to increase with concentration until saturation after 100 µg/mL. We believe that this is due to a limitation in nanoparticle uptake by the cell, that was confirmed with flow cytometry as a saturation in the mean SSC (data not shown).

Nanoparticle Radiosensitization

The toxicity data above indicates that a concentration of 50 µg/mL is suitable for the *in vitro* radiosensitization experiments. The surviving fraction of 9L cells irradiated at 150 kVp with and without exposure to NPs at a concentration of 50 µg/mL is shown in Figure 6. The high-Z of thulium-based nanoparticles (Z = 69) creates a greater likelihood of secondary electron production on interaction with X-rays which is expected to lead to an enhancement of the radiation-induced damage to the cells through increased energy deposition. The behaviour of the cell survival curve can be described by equation 1 above. The parameters of the linear quadratic model that describe the trend are given in Table 1 for both the case of radiation alone (cells only) and 9L cells with the addition of thulium oxide nanoparticles.

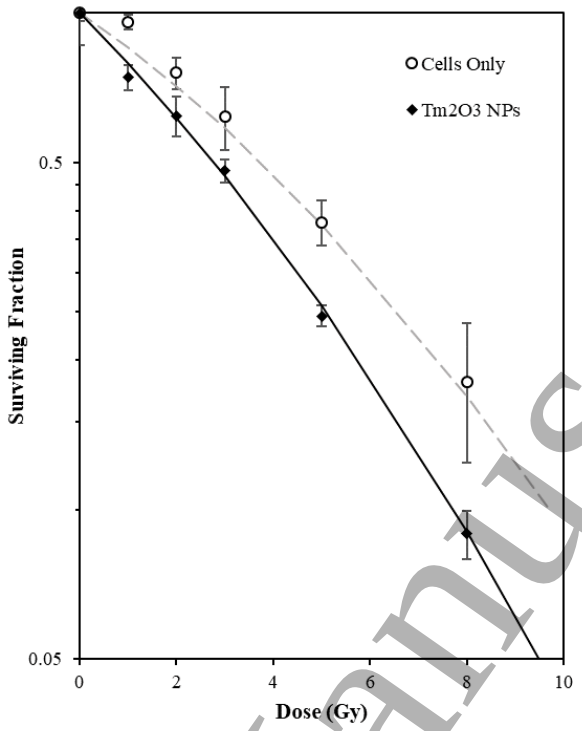

Figure 6: Clonogenic survival of 9L cells irradiated at 150 kVp in the presence (solid line) and absence (dotted line) of Tm_2O_3 nanoparticles

With the addition of the nanoparticles, the linear component of the trend, α, is greater. According to Jones *et al* 2001 this corresponds to an increase in the probability per dose of a single radiation interaction resulting in cell death rather than the necessity of two interactions for a lethal event that is represented by the quadratic component, β.

The cell sensitivity enhancement ratio (SER) at 10% SF was found to be 1.32 for thulium oxide nanoparticles when considering the only effect of the radiation enhancement due to the nanoparticle, and not including intrinsic toxicity. This is comparable with other nano-structured ceramics considered for radiotherapy such as tantalum oxide, with SER of 1.33 irradiated with 10 MV X-rays (Brown *et al* 2014).

Treatment	α (Gy^{-1})	β (Gy^{-2})
9L Cells Only	0.15 ± 0.03	0.009 ± 0.003
9L cells with Tm_2O_3 NPs	0.22 ± 0.02	0.010 ± 0.003

Table 1: Summary of Radiobiological parameters, excluding the intrinsic toxicity of the thulium nanoparticles.

Figure 7 shows an assessment of DNA damage in the form of double-strand DNA breaks (green) in 9L cells using a Mouse Anti-γ-H2AX IgG1 primary antibody that was introduced to fixed

cells 15 mins after irradiation with 150 kVp X-rays *in vitro*. A single dose of 8 Gy was considered for the case with and without 50 µg/mL Tm_2O_3 NPS, and the formation of foci induced by the secondary Alexa Fluor 488 conjugated goat anti-mouse IgG1 antibody which was detected at 448 nm using a Leica DMi8 microscope.

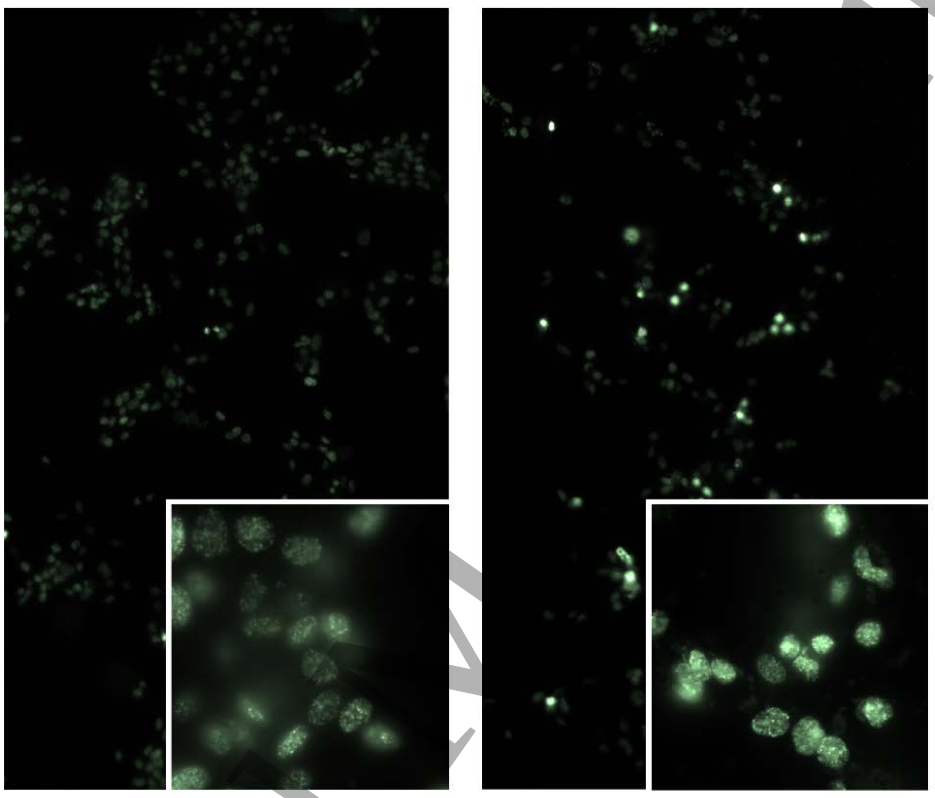

Figure 7: Double-stranded DNA breaks in 9L cells following *in vitro* irradiation with 8 Gy 150 kVp X-rays, using γ-H2AX (green). 8 Gy without nanoparticles (A) and 8 Gy with thulium nanoparticles (B), both shown with dry 20x objective in the primary panel and 40x objective in the sub-panel.

The formation of γ-H2AX foci at 8 Gy tends to increase in the presence of nanoparticles. This is evident in Figure 7 by the greater occurrence of enlarged foci that corresponds to clustered, more numerous incidences of double-strand DNA breaks. A greater density of foci was observed to localize near larger conglomerates of nanoparticles within the cell, leading to larger and denser foci localized within these regions of the nucleus. The site-specific nanoparticle enhanced damage is believed to responsible for the improvement in the 9L cell treatment observed in Figure 6.

CT Contrast Enhancement

The average CT number (HU) was measured using ImageJ for various concentrations of thulium oxide in DPBS, and the values were compared with common substances or tissues found in the

body (Figure 8). Mean CT numbers of the NP solutions were obtained with ImageJ and errors represent the standard deviation of the mean. Even low concentrations of the thulium-based particles (0.25-0.5 mg/mL) will begin to produce contrast above normal brain tissue with a HU of 27. Above 10 mg/mL, the nanoparticles begin to aggregate. This leads to greater error in the measured average CT number.

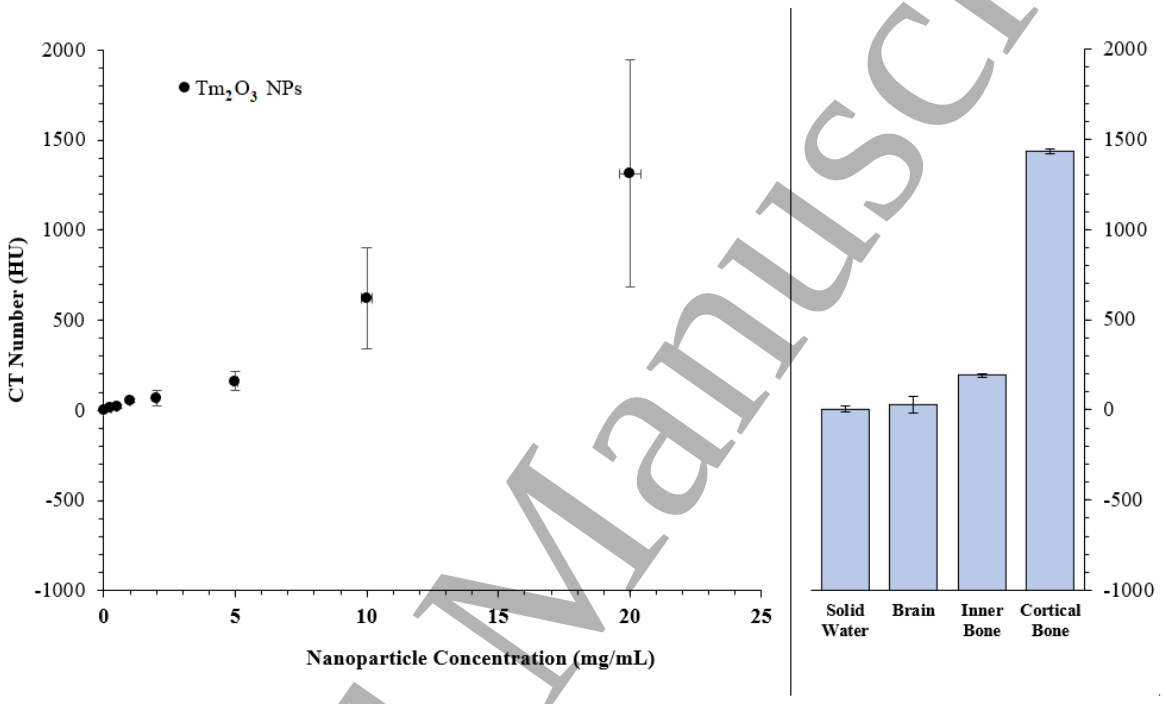

Figure 8: Average CT number measured for various concentrations of Tm_2O_3 nanoparticles, compared non-linearly to CT numbers of common materials found in the body as provided by a 467 Gammex Tissue Calibration Phantom.

In a separate *in vivo* study, thulium nanoparticles (40 µg or 2 µL and concentration of 20 mg/mL) were injected into the caudate nucleus of 9- to 10-week-old Fischer rats in order to target the brain cancer at day 12 following tumour implantation. In Figure 9, the evolution of the nanoparticles' uptake and position is shown.

In Fig. 9A, the thulium nanoparticles are initially localized around the injection point at 5 mins following injection. By 10 mins, the nanoparticles have distributed around and inside the tumour volume (Fig. 9B) and by 25 mins, the nanoparticles are cleared from the tumour (Fig. 9C). The rodents monitored to 24 hrs showed no trace of the thulium particles. We also observed no accumulation within the kidneys from injection up until our maximum observing time of 36 hrs following the nanoparticle injection. Some nanoparticles such as gold or gadolinium are known to stay in the cancer for longer periods of time (Rogosnitzky *et al* 2016). We find that the fast clearance of these nanoparticles from the cancer may be beneficial in reducing the amount of

residual high-Z material in the brain. No adverse effects to rodent behaviour or health was observed up to 3 days following nanoparticle injection. Euthanasia of rats occurred as planned up to day 17.

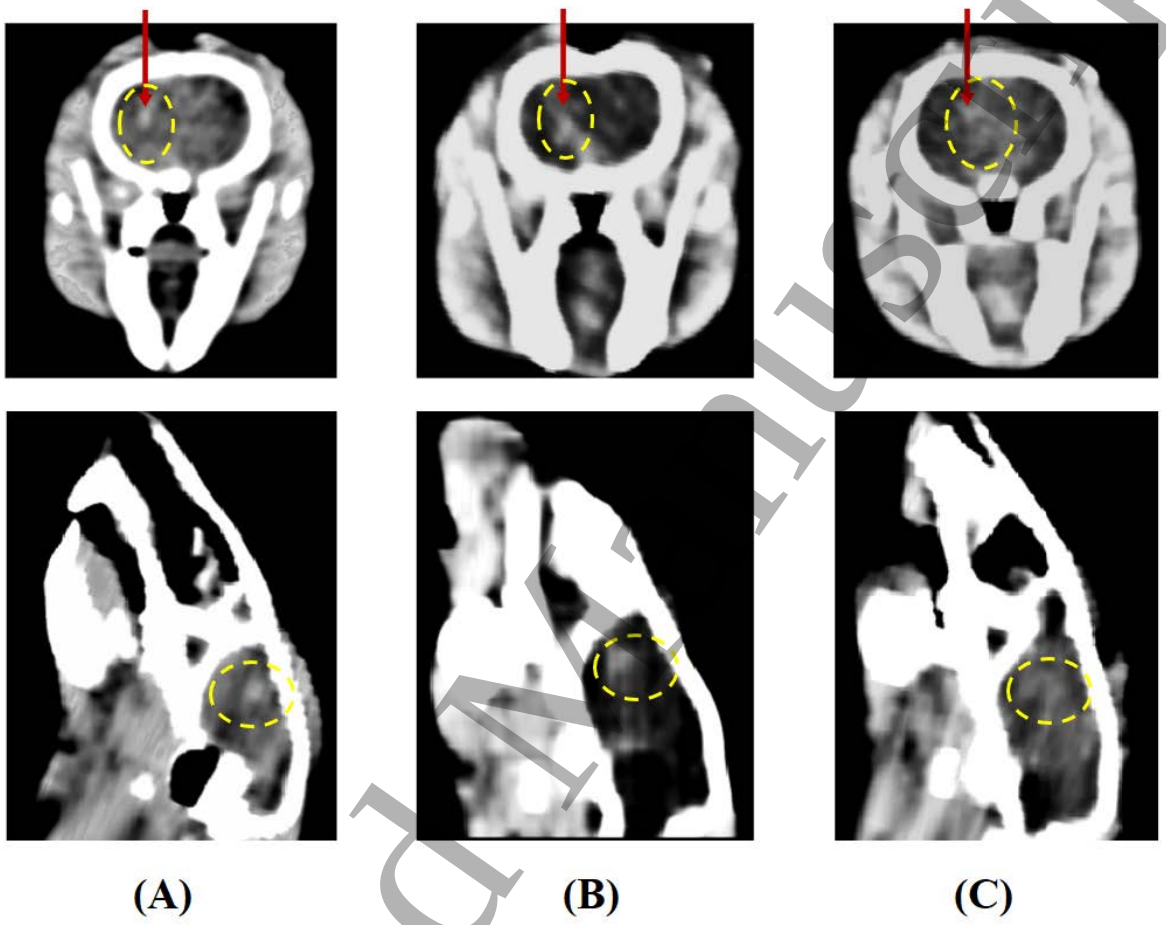

Figure 9: Transverse and sagittal CT images of 3 separate Fischer rats bearing 9L gliosarcoma brain tumours 5 min (A), 10 min (B), and 25 mins (C) after injection of 2 µL of 20 mg/mL thulium oxide nanoparticles. Injection route is shown with red arrows, and the tumour region of interest shown in yellow.

CONCLUSION

This work presents the first use of thulium-based nanoparticles for biological applications. We have identified their potential in treatment and diagnosis of radioresistant brain cancers with a 9L gliosarcoma brain cancer model, both *in vitro* and *in vivo*.

We have shown that the Tm_2O_3 nanoparticles are well internalized into the brain cancer cells. Their size of 40 nm and spherical or elongated shape can allow the particles a greater likelihood of interaction with the cell membrane and to be internalized well into cells (Kinnear *et al* 2017).

They do however, show a slight toxicity towards them to induce at maximum 40% survival after 3 weeks following an initial 24 hr exposure with concentrations up to 500 µg/mL.

These thulium nanoparticles are capable of causing radio-sensitization with 150 kVp X-rays with just 50 µg/mL. Furthermore, high concentrations are not required during CT or radiotherapy, with only 40 µg capable of producing contrast of the tumour against normal brain with CT. The faster clearance from the tumour site also may be beneficial for reducing nanoparticle accumulation in the brain, and the lack of thulium present in the kidneys implies potentially less danger for the development of NSFs.

Our findings indicate thulium nanoparticles are good candidates for image-guided radiotherapies. We have successfully shown radiosensitization of tumour cells for a kilovoltage radiation field, which motivates thulium nanoparticles to be considered for novel kilovoltage therapies treatment of melanomas (surface cancers) or novel therapies for brain cancer such as synchrotron radiation treatments, including microbeam radiation therapy (MRT).

There is need to investigate cancer-specific targeting with thulium oxide nanoparticles. Further study into nanoparticle induced cancer cell toxicity both *in vitro* and *in vivo* is required, as there is limited evidence here for normal tissue tolerance from the *in vivo* data. For the time being, the thulium oxide nanoparticles have no designed cancer cell-specificity. We directly injected the nanoparticles to the site; however the ability of the nanoparticles to cross the blood brain barrier must also be assessed. In future, the steps towards personalised medicine can be followed to modify nanoparticles for the delivery and specific uptake to cancer cells through changes to size, shape, coating and payload development (Nguyen, 2011). However, tumours of various types and sizes tend to have different interactions with nanoparticles and require careful consideration of nanoparticle properties both for diagnostics and treatments. For this reason, further study into more cell lines both cancerous and normal must be considered *in vivo and in vitro* to determine uptake and stability factors for the raw thulium oxide nanoparticle we have investigated here and any modified targeted nanoparticles.

ACKNOWLEDGEMENTS

We acknowledge the Prince of Wales Hospital, the Illawarra Health and Medical Research Institute (IHMRI), the UOW Electron Microscopy Centre and the UOW Animal Ethics Committee and Animal House. We acknowledge the financial support of the Australian Government Research Training Program Scholarship, and Australian National Health & Medical Research Council (APP1084994 and APP1093256).

REFERENCES

Ashton JR, West JL, & Badea CT, 2015. In vivo small animal micro-CT using nanoparticle contrast agents. Frontiers in Pharmacology, 6, 256.

Australian Institute of Health and Welfare, 2017. Brain and other central nervous system cancers. Cat. no. CAN 106. Canberra: AIHW.

Barbalat Y, Velez MC, Sayegh CI, Chung DE, 2016 Evidence of the efficacy and safety of the thulium laser in the treatment of men with benign prostatic obstruction. Therapeutic Advances in Urology. 8(3):181-191.

Barnett GC, West CM, Dunning AM, Elliott RM, Coles CE, Pharoah PD, Burnet NG, 2009. Normal tissue reactions to radiotherapy: towards tailoring treatment dose by genotype. Nat Rev Cancer; 9:134-1.

Barth RF, 1998. Rat brain tumor models in experimental neuro-oncology: the 9L, C6, T9, F98, RG2 (D74), RT-2 and CNS-1 gliomas. J Neurooncol. Jan; 36(1):91-102.

Baskar R, Lee KA, Yeo R, Yeoh KW, 2012. Cancer and Radiation Therapy: Current Advances and Future Directions. Int J Med Sci 9(3):193-199.

Bogusz K, Tehei M, Stewart C, McDonald M, Cardillo D, Lerch M, Corde S, Rozenfeld A, Liu HK and Konstantinov K, 2014. Synthesis of potential theranostic system consisting of methotrexate-immobilized (3-aminopropyl)trimethoxysilane coated α- Bi2O3 nanoparticles for cancer treatment. RSC Advances, 4 (46), 24412-24419

Borchert H, Shevchenko E, Robert A, Mekis I, Kornowski A , Grübel G, Weller H, 2005. Determination of nanocrystal sizes: a comparison of TEM, SAXS, and XRD studies of highly monodisperse CoPt3 particles. Langmuir. 1;21(5):1931-6., 21, 1931 .

Briggs A, Corde S, Oktaria S, Brown R, Rozenfeld A, Lerch M, Konstantinov K and Tehei M, 2013. Cerium oxide nanoparticles: influence of the high-Z component revealed on radioresistant 9L cell survival under X-ray irradiation. Nanomedicine, 9 (7), 1098-1105.

Brown R, Tehei M, Oktaria S, Briggs A, Stewart C, Konstantinov K, Rosenfeld A, Corde S, Lerch M, 2014. High-Z Nanostructured Ceramics in Radiotherapy: First Evidence of Ta2O5-Induced Dose Enhancement on Radioresistant Cancer Cells in an MV Photon Field. Particle and Particle Systems Characterization 31 (4): 500–505.

Brown R, Corde S, Oktaria S, Konstantinov K, Rosenfeld A, Lerch M, Tehei M, 2017. Nanostructures, concentrations and energies: an ideal equation to extend therapeutic efficiency on radioresistant 9L tumor cells using Ta_2O_5 ceramic nanostructured particles. Biomedical Physics & Engineering Express, 3 (1).

European Medicines Agency, 2017. PRAC concludes assessment of gadolinium agents used in body scans and recommends regulatory actions, including suspension for some marketing authorisations. Review finds evidence of gadolinium deposits in the brain after MRI body scans but no signs of harm. EMA/157486/2017.

http://www.ema.europa.eu/docs/en_GB/document_library/Press_release/2017/03/WC500223209.pdf

Goldman LW, 2007. Principles of CT and CT Technology, J. Nucl. Med. Technol. 35 (3) 115-128.

Hainfeld JF, Slatkin DN, Smilowitz HM, 2004. The use of gold nanoparticles to enhance radiotherapy in mice, Phys Med Biol. 49(18): N309-15.

Hainfeld JF, Dilmanian FA, Slatkin DN, Smilowitz HM, 2008. Radiotherapy enhancement with gold nanoparticles. J Pharm Pharmacol. 2008 Aug;60(8):977-85.

Haume K, Rosa S, Grellet S, Śmiałek MA, Butterworth KT, Solov'yov AV, Prise KM, Golding J and Mason NJ, 2016. Gold nanoparticles for cancer radiotherapy: a review. Cancer Nanotechnology.7(1):8.

Havron A, Davis MA, Seltzer SE, Paskins-Hurlburt AJ, and Hessel SJ, 1980. Heavy Metal Particulate Contrast Materials for Computed Tomography of the Liver; Journal of Computer Assisted Tomography, 4(5):642.

Heiligtag F and Niederberger M, 2013. Materials Today Volume 16, Numbers 7/8 July/August R.

Hubbel JH and Seltzer SM, 1995. Tables of X-Ray Mass Attenuation Coefficients and Mass Energy-Absorption Coefficients 1 keV to 20 MeV for Elements Z=1 to 92 and 48 Additional Substances of Dosimetric Interest. NISTIR 5632. (http://physics.nist.gov/PhysRefData/XrayMassCoef/cover.html).

Ivashkevich A, Redon CE, Nakamura AJ, Martin RF, Martin OA, 2012. Use of the c-H2AX assay to monitor DNA damage and repair in translational cancer research. Cancer Letters 327, 123–133.

Jones L, Hoban P and Metcalfe P, 2001. The Use of the Linear Quadratic Model in Radiotherapy: A Review. Australasian Physical & Engineering Sciences in Medicine, Vol. 24, No. 3, 132-146.

Kelley K, Knisely J, Symons M, Ruggieri R, 2016. Radioresistance of Brain Tumors. *Cancers*, 8, 42: p1-28.

Kinnear C, Moore TL, Rodriguez-Lorenzo L, Rothen-Rutishauser B, Petri-Fink A, 2017. Form Follows Function: Nanoparticle Shape and Its Implications for Nanomedicine. Chem Rev. 117(17):11476-11521.

Koehler WC, Cable JW, Wollan EO & Wilkinson MK,1962. Phys. Rev. B 126, pp1672.

Kotb S, Detappe A, Lux F, Appaix F, Barbier EL, Tran V, Plissonneau M, Gehan H, Lefranc F, Rodriguez-Lafrasse C, Verry C, Berbeco R, Tillement O, Sancey L., 2016. Gadolinium-Based Nanoparticles and Radiation Therapy for Multiple Brain Melanoma Metastases: Proof of Concept before Phase I Trial, Theranostics 6(3): 418-427.

Lohrke J, Frenzel T, Endrikat J, Alves FC, Grist TM, Law M, Lee JM, Leiner T, Li KC, Nikolaou K, Prince MR, Schild HH, Weinred JC, Yoshikawa K, Pietsch H, 2016. 25 Years of Contrast-Enhanced MRI: Developments, Current Challenges and Future Perspectives. Adv Ther 33:1–28.

Lusic H, Grinstaff MW., 2013, X-Ray Computed Tomography Contrast Agents. Chemical reviews. 113(3):pp 1641–1666.

Lutterotti L, Matthies S, Wenk HR, Schultz AJ and Richardson J, 1997. Combined texture and structure analysis of deformed limestone from neutron diffraction spectra, J. Appl. Phys., 81[2], 594-600.

Maggiorella L, Barouch G, Devaux C, Pottier A, Deutsch E, Bourhis J, Borghi E, Levy L, 2012. Nanoscale radiotherapy with hafnium oxide nanoparticles, Future Oncology; London 8.9: 1167-81.

Malaise EP, Fertil B, Chavandra N and Guichard M, 1986. Distribution of radiation sensitivities for human tumour cells of specific histological types. Comparison of in vitro to in vivo data. Int J Radiat Oncol Biol Phys 12: 617-624.

McDonald M, Oktaria S, Konstantinov K, Rosenfeld A, Lerch M, Corde S, Tehei M, 2018. Radiosensitisation enhancement effect of BrUdR and Ta2O5 NSPs in combination with 5-Fluorouracil antimetabolite in kilovoltage and megavoltage radiation. Biomed. Phys. Eng. Express 4 034001

McKinnon S, Engels E, Tehei M, Konstantinov K, Corde S, Oktaria S, Incerti S, Lerch M, Rosenfeld A, Guatelli S, 2016. Study of the effect of ceramic Ta2O5 nanoparticle distribution on cellular dose enhancement in a kilovoltage photon field. Physica Medica: European Journal of Medical Physics, 32 (10), 1216 – 1224.

McQuaid H, Muir MF, Taggart LE, McMahon SJ, Coulter JA, Hyland WB, Jain S, Butterworth KT, Schettino G, Prise KM, Hirst DG, Botchway SW & Currell FJ, 2016. Imaging and radiation effects of gold nanoparticles in tumour cells. Scientific Reports volume 6, Article number: 19442

Nowotny R, XmuDat 1998, Photon attenuation data on PC, Version 1.0.1.

Nguyen KT, 2011. Targeted Nanoparticles for Cancer Therapy: Promises and Challenges. J Nanomedic Nanotechnol 2:5:103e

Ostrom QT, Gittleman H, de Blank PM, Finlay JL, Gurney JG, McKean-Cowdin R, Stearns DS, Wolff JE, Liu M, Wolinsky Y, Kruchko C, Barnholtz-Sloan JS, 2015. American Brain Tumor Association Adolescent and Young Adult Primary Brain and Central Nervous System Tumors Diagnosed in the United States in 2008-2012, Neuro-Oncology 18:i1–i50.

Pereira A F, Silva J F., Gouveia-Neto A. S. & Jacinto C, 2017. 1.319 μm excited thulium doped nanoparticles for subtissue thermal sensing with deep penetration and high contrast imaging. Sensors Actuators B Chem. 238, 525–531.

Poludniowski G, Landry G, DeBlois F, Evans PM, Verhaegen F, 2009. SpekCalc: a program to calculate photon spectra from tungsten anode x-ray tubes. Phys Med Biol. 7;54(19):N433-8.

Retif P, Pinel S, Toussaint M, Frochot C, Chouikrat R, Bastogne T, Barberi-Heyob M., 2015. Nanoparticles for Radiation Therapy Enhancement: the Key Parameters. Theranostics. 5(9):1030-1044.

Rogosnitzky M, Branch S, 2016 Gadolinium-based contrast agent toxicity: a review of known and proposed mechanisms. Biometals; 29:365-376.

Shang L, Nienhaus K and Nienhau GU, 2014. Engineered nanoparticles interacting with cells: size matters. Journal of Nanobiotechnology, 12:5.

Sidorowicz A, Wajler A, Weglarz H, Jach K, Orlinski K, Olszyna A, 2016. Thulium Oxide Nanopowders Obtained by Precipitation. Int. J. Appl. Ceram. Technol., 13 [2] 302–307.

Sinharay S, and Pagel MD, 2016. Advances in Magnetic Resonance Imaging Contrast Agents for Biomarker Detection. Annu. Rev. Anal. Chem. 9:95–115.

Stewart C, Konstantinov K, McKinnon S, Guatelli S, Lerch M, Rosenfeld A, Tehei M, Corde S, 2016. First proof of bismuth oxide nanoparticles as efficient radiosensitisers on highly radioresistant cancer cells. Physica Medica: an international journal devoted to the applications of physics to medicine and biology, 32 (11), 1444-1452.

Zhang WX, Pan YB, Zhou J, Liu WB, Li J, Zou YW, Wei Z, 2011. Preparation and characterization of transparent Tm:YAG ceramics. Ceramics International – CERAM INT. 37. 1133-1137.